Geometry-based tunability enhancement of flexible thin-film varactors

Article (Accepted Version)

Geometry based tunability enhancement of flexible thin-film varactors

S. Knobelspies, C. Gonnelli, C. Vogt, *Student Member, IEEE*, A. Daus, N. Münzenrieder, *Member, IEEE* and Gerhard Tröster, *Senior Member, IEEE*

***Abstract*—In this work, flexible voltage-controlled capacitors (varactors) based on an amorphous Indium-Gallium-Zinc-Oxide (a-IGZO) semiconductor are presented. Two different varactor designs and their influence on the capacitance tuning characteristics are investigated. The first design consists of a top electrode finger structure which yields a maximum capacitance tunability of 6.9 at 10 kHz. Secondly, a novel interdigitated varactor structure results in a maximum tunability of 93.7 at 100 kHz. The design- and frequency dependencies of the devices are evaluated through C-V measurements. Furthermore, we show bending stability of the devices down to a tensile radius of 6 mm without altering the performance. Finally, a varactor is combined with a thin-film resistor to demonstrate a tunable RC-circuit for impedance matching and low-pass filtering applications. The device fabrication flow and material stack is compatible with standard flexible thin-film transistor fabrication which enables parallel implementation of analog or logic circuitry and varactor devices.**

***Index Terms*—Varactor, Indium-Gallium-Zinc-Oxide (IGZO), flexible electronics, thin-film technology, MOS.**

I. Introduction

VARACTORS are one of the key components for tunable filters [1] and voltage controlled oscillators (VCOs) [2], which find application in analog signal processing and devices such as wearable sensors [3], amplifiers [4], RFID tags [5] and wireless communication systems. State-of-the-art technologies realize tunable capacitors either by MEMS based mechanical changes in geometry [6], by inversion type metal-oxide-semiconductor (MOS) stacks [2] or a change in the dielectric constant of the insulating material in metal-insulator-metal stacks, e.g. implemented by ferroelectric [7] or liquid crystal [8] type dielectrics. Regarding the field of flexible electronics, the two latter ones can be realized, but yield tunabilities smaller than 0.3 [7], [8]. Here, we present two designs of amorphous Indium-Gallium-Zinc-Oxide (a-IGZO) based thin-film varactors fabricated on free-standing Polyimide foil, which are realized in a metal-oxide-semiconductor-metal stack. To the best of our knowledge, this is the first demonstration of a flexible thin-film varactor based on an amorphous oxide semiconductor. A-IGZO is chosen, since it has received noteworthy attention due to its electrical properties, such as an electron mobility > 10 $cm^2V^{-1}s^{-1}$ and the possibility for low temperature deposition [9]. Despite partly consisting of rare earth materials, a-IGZO based electronics became commercially viable [10]. The presented fabrication flow can be directly implemented into thin-film transistor technology without the need of additional materials or processes. Our varactor approach utilizes the semiconductor transition from depletion to accumulation, resulting in effective geometry change of the capacitor dimensions. The first device consists of a top electrode finger structure with a capacitance tunability of 6.9. Secondly, an interdigitated varactor design is implemented, increasing the tunability to 93.7. We show remarkable capacitance tunabilities for frequencies up to 1 MHz and the varactor integration in an RC-circuit for impedance matching and low-pass filtering. These devices open the way to fully integrated wireless and flexible devices and applications such as intrabody communication [11], AM-FM conversion [12], active phase shifters [13] or analog signal processing.

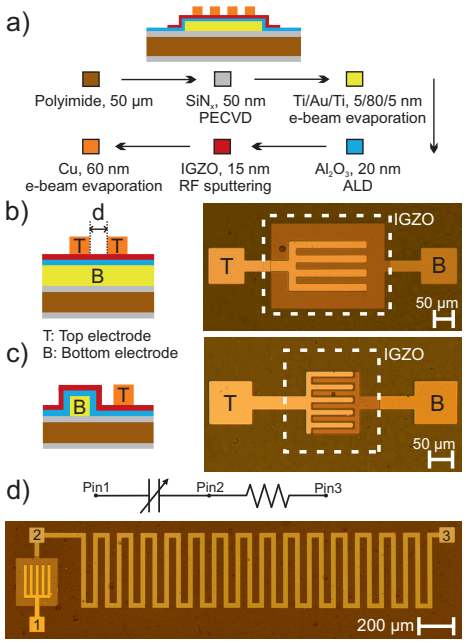

Fig. 1. a) Schematic fabrication flow. b) Schematic device cross section and micrograph of the top electrode finger (TE) varactor, where d indicates the finger spacing. c) Schematic device cross section and a micrograph of the interdigitated (ID) varactor. d) Equivalent circuit diagram of the RC-circuit and a microscopic picture of the fabricated device.

This work was supported by a grant from the Swiss National Science Foundation (SNSF), Switzerland through the project "WISDOM", Grant No. 200021E-160347/1.

S. Knobelspies, C. Gonnelli, C. Vogt, A. Daus, N. Münzenrieder and G. Tröster are with the Institute for Electronics, Swiss Federal Institute of Technology Zurich (ETH Zurich), Zurich 8092, Switzerland,
(e-mail: stefan.knobelspies@ife.ee.ethz.ch).
N. Münzenrieder is also with the Sensor Technology Research Center, School of Engineering and Informatics, University of Sussex, Falmer, Brighton BN1 9QT, United Kingdom.

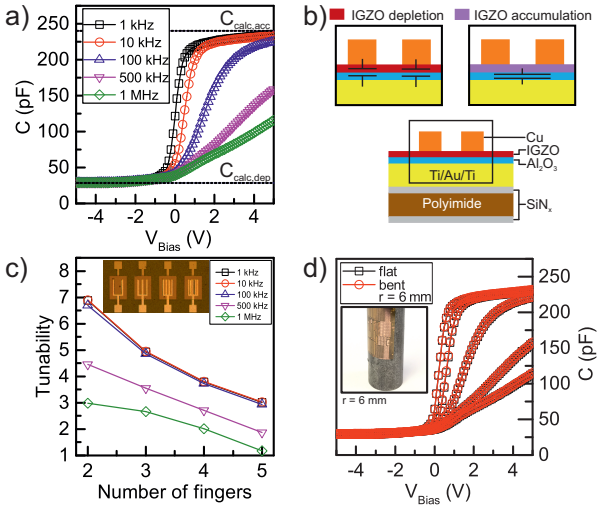

Fig. 2. a) Exemplary capacitance-voltage (C-V) characteristic of a TE varactor with two fingers at five frequencies ranging from 1 kHz to 1 MHz. The dashed lines indicate the calculated capacitance values in depletion and accumulation. b) Schematic device cross section highlighting the change in the effective capacitance area A and thickness t of the capacitor due to the semiconductor transition from depletion (left) to accumulation (right). c) Relation between number of fingers and the tunability of the TE varactor at the same frequencies as in (a). The dimension of the bottom electrode for all devices is constant. The analyzed devices are shown in the inset. d) C-V characteristic of the TE varactor while being flat and bent to a tensile radius of 6 mm. The measurements are performed at the same frequencies as in (a). A photograph of the devices attached to a cylindrical metal rod is presented in the inset.

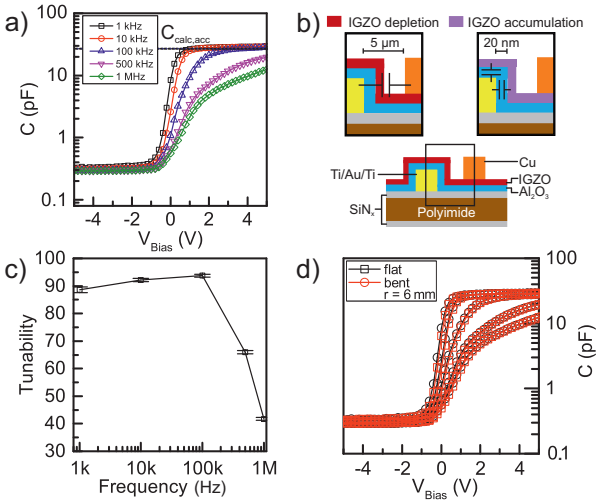

Fig. 3. a) Exemplary log-scale capacitance-voltage (C-V) characteristic of the ID varactor at five different frequencies ranging from 1 kHz to 1 MHz. The calculated capacitance in accumulation is indicated by the dashed line. b) Schematic device cross section highlighting the change in t from the micrometer- to the nanometer range due to the semiconductor transistion from depletion (left) to accumulation (right). c) Tunability of the ID varactor in relation to the frequency. d) C-V characteristic of the ID varactor while being flat and bent to a tensile radius of 6 mm. The measurements are performed at the same frequencies as in (a).

II. Device Structure and Fabrication

Fig. 1a shows the fabrication flow, which is comparable to our previous work [14], [15]. The devices are fabricated on free-standing 50 µm thick Polyimide foil. First, the substrate is cleaned by sonication in Acetone and 2-Propanol for 5 minutes each, followed by baking at 200 °C for 24 hours to remove residual solvents. Then, 50 nm SiN_x is deposited on both sides by plasma-enhanced chemical vapor deposition (PECVD) at 150 °C to promote the adhesion for the following layers. Subsequently, the bottom electrode, consisting of Ti/Au/Ti (5/80/5 nm) for the varactors or 30 nm of Ti for the RC-circuits is electron beam evaporated and patterned by lift-off. A 20 nm Al_2O_3 insulator layer is grown by atomic layer deposition (ALD) at 150 °C, followed by a 15 nm thick a-IGZO layer deposited by RF magnetron sputtering at room temperature. The semiconductor is structured into islands and vias are formed in the insulator, both by wet etching. Next, a 60 nm thick Cu layer is deposited by electron beam evaporation and structured by lift-off, forming the top electrode.

For the top electrode finger structure (TE varactor), as presented in Fig. 1b, the area of the bottom electrode is kept constant (320 µm x 240 µm) while increasing the number of fingers which are uniformly distributed. This results in a change of the finger spacing d from 100 µm to 10 µm. Fig. 1c presents the interdigitated varactors (ID varactor). Here, the finger spacing is 5 µm with a finger width of 10 µm. In addition, RC-circuits are fabricated, which are shown by the equivalent circuit diagram, as well as a microscopic picture in Fig. 1d. The serpentine structure is used to obtain a thin-film resistor together with a tunable TE varactor.

III. Results and Discussion

The devices are characterized under ambient conditions using a semiconductor device analyzer (Agilent B1500A, ac impedance measurement with an ac oscillation voltage V_{AC} = 200 mV, employing the RC parallel model). Capacitance-voltage (C-V) measurements of the varactors and impedance spectroscopy of the RC-circuit are conducted. The performance of the varactors is benchmarked by the capacitance tunability, which is calculated by:

$$\text{Tunability} = (C_{max} - C_{min})/C_{min} \quad (1)$$

A. Top electrode finger (TE) varactors

In the following, the influence of finger distance, as well as number of fingers, on the tunability of the varactor is investigated. The capacitance C of the devices can be calculated by the parallel plate capacitor equation

$$C = \epsilon_0 \cdot \epsilon_r \cdot A/t, \quad (2)$$

where ϵ_0 is the vacuum permittivity, ϵ_r the relative dielectric constant, A the effective capacitance area and t the distance between the two electrodes.

Fig. 2a shows the C-V plot of a varactor with two fingers. The capacitance rises with increasing bias voltage, which is attributed to the semiconductor transition from depletion to accumulation. In this case the a-IGZO, which is covered by the top electrode fingers as well as the fingers' surrounding area, becomes conductive [16]. It acts as an electrode material thereby increasing the effective capacitance area A. Additionally, the effective t between both electrodes is reduced, which is in agreement with the well-known MOS varactor principle [2], [17]. The lower dashed line indicates the calculated

capacitance in depletion $C_{calc,dep}$, only taking the overlap area between top and bottom electrode into account. The upper dashed line shows the calculation in accumulation $C_{calc,acc}$, assuming that the whole a-IGZO island becomes conductive and the effective t decreases to the thickness of the Al_2O_3 layer. The calculations are in agreement with the measurements showing deviations smaller than 4 % using $\epsilon_{r,IGZO} = 16$ [18] and $\epsilon_{r,Al_2O_3} = 7$ [19]. The schematic device cross section in Fig. 2b highlights the change in A and t in the depletion and accumulation case. As the dominating effect (i.e. the change of A) relies on the expansion of the conductive a-IGZO area between the electrode fingers, the relation between number of fingers and tunability is investigated in Fig. 2c, while keeping the size of the bottom electrode constant. The highest tunability of 6.9 at 10 kHz is achieved for the lowest number of fingers, which means that the maximum gap of 100 µm between two fingers is becoming conductive. A lower number of fingers also lowers the capacitance in depletion contributing to the presented tunability dependence, while the accumulation capacitance stays constant. Additionally, a frequency dispersion of the C-V characteristics and therefore of the tunability is visible, which is in agreement with observations of the gate capacitance of a-IGZO TFTs [20]. This can be attributed to the a-IGZO resistance in accumulation and the fact, that for increasing frequency, the charging and discharging of the trap states can not follow the applied voltage and their contribution to the semiconductor capacitance decreases [21]. Fig. 2d compares the varactor performance in flat and bent condition. For the bending experiments, the devices are attached to a cylindrical metal rod with a radius of 6 mm (see inset). The change in the C-V characteristics can be considered negligible, which is in agreement to our previous work [22]. By I-V measurements, we identified the leakage current being always below 20 pA.

B. Interdigitated (ID) varactors

In this part, the C-V characteristic, tunability and performance under bending of the ID varactor are investigated.
Fig. 3a displays the C-V plot of the above described ID device. In contrast to the device presented in section A, the dominant effect contributing to the capacitance change is the modulation of t, when the semiconductor becomes conductive, which is highlighted in the schematic cross section in Fig. 3b. In depletion, t is determined by the lateral spacing between the bottom and the top electrode (5 µm). The transition into accumulation reduces the effective t to the Al_2O_3 thickness (20 nm). The dashed line in Fig. 3a indicates the calculated expected capacitance in accumulation $C_{calc,acc}$, assuming that the whole IGZO island is conductive. The frequency dispersion and the leakage current are similar to the above described TE varactor. Fig. 3c presents the extracted tunabilities of the ID varactor at different measurement frequencies. The maximum tunability of 93.7 is achieved at 100 kHz while the device still retains a tunability of 41.7 at the highest frequency of 1 MHz. The results in Fig. 3d show, that the C-V characteristic of the ID varactor is also only insignificantly affected by the mechanical bending.

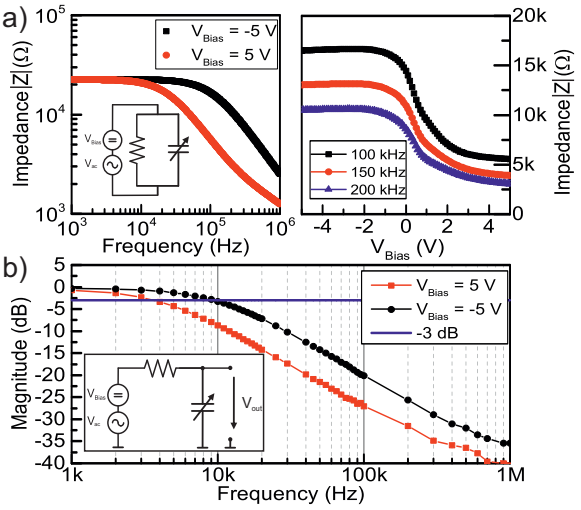

Fig. 4. a) (left) Impedance spectroscopy of the RC parallel circuit (equivalent curcuit shown in the inset) for $V_{Bias} = -5$ V and 5 V. (right) Impedance |Z| in relation to the applied bias voltage V_{Bias} at 100 kHz, 150 kHz and 200 kHz. b) Bode magnitude plot of the tunable low-pass filter at $V_{Bias} = -5$ V and 5 V.

C. Tunable RC-circuit

In this section, possible applications of the varactors in an integrated tunable RC-circuit (see Fig. 1d) are presented. First, a TE varactor is used in parallel to a resistor of 21.7 kΩ (see inset Fig. 4a) and excited by an ac voltage of 200 mV in superposition with a variable dc voltage V_{Bias}. Fig. 4a (left) shows the impedance versus frequency plot for two exemplary V_{Bias} of −5 V and 5 V. To investigate the tuning compatibilities, the impedance values at 100 kHz, 150 kHz and 200 kHz for bias voltages between −5 V and 5 V are plotted in Fig. 4a (right). In this configuration, the RC-circuit can be used for impedance matching. Fig. 4b shows the varactor application in a tunable RC-filter with the same ac and dc settings as described above. A TE varactor is used in series to a thin-film resistor, as indicated in the inset. Depending on the applied V_{Bias}, the filter characteristics, and therefore the cut-off frequency can be tuned accordingly.

IV. Conclusion

In summary, we presented mechanically flexible a-IGZO based thin-film varactors fabricated on a free-standing Polyimide foil, that are based on a metal-oxide-semiconductor-metal structure. Devices with a top electrode finger (TE) design achieved tunabilities up to 6.9 at 10 kHz and a novel interdigitated (ID) varactor design increased the tunability up to a value of 93.7 at 100 kHz. Supported by calculations, the measurements showed how the device structure, geometry and frequency influence the tunability. Furthermore, the performance of both devices is not altered while being bent to a tensile radius of 6 mm. Finally, we presented two varactor applications in a tunable RC-circuit for impedance matching, as well as a tunable low-pass filter. Future work should be focused on investigating the high frequency performance above 1 MHz.

REFERENCES

[1] A. R. Brown and G. M. Rebeiz, "A Varactor-Tuned RF Filter," *IEEE Trans. Microw. Theory Tech.*, vol. 48, no. 7, pp. 1157–1160, 2010, doi: 10.1109/22.848501.

[2] P. Andreani and S. Mattisson, "On the Use of MOS Varactors in RF VCOs," *IEEE J. Solid-State Circuits*, vol. 35, no. 6, pp. 905–910, 2000, doi: 10.1109/4.845194.

[3] B. E. Horton, S. Schweitzer, A. J. DeRouin, and K. G. Ong, "A varactor-based, inductively coupled wireless pH sensor," *IEEE Sens. J.*, vol. 11, no. 4, pp. 1061–1066, 2011, doi: 10.1109/JSEN.2010.2062503.

[4] S. Chatterjee, Y. Tsividis, and P. Kinget, "0.5-V analog circuit techniques and their application in OTA and filter design," *IEEE J. Solid-State Circuits*, vol. 40, no. 12, pp. 2373–2387, 2005, doi: 10.1109/JSSC.2005.856280.

[5] U. Karthaus and M. Fischer, "Fully Integrated Passive UHF RFID Transponder IC with 16.7- W Minimum RF Input Power," *IEEE J. Solid-State Circuits*, vol. 38, no. 10, pp. 1602–1608, 2003, doi: 10.1109/JSSC.2003.817249.

[6] N. A. Ramli, T. Arslan, N. Haridas, and W. Zhou, "Design and simulation of a high tuning range MEMS digital varactor using SU-8," *Symp. Des. Test, Integr. Packag. MEMS/MOEMS, DTIP 2016*, pp. 1–5, 2016, doi: 10.1109/DTIP.2016.7514842.

[7] Y. Shen, S. Ebadi, P. Wahid, and X. Gong, "Tunable and flexible Barium Strontium Titanate (BST) varactors on Liquid Crystal Polymer (LCP) substrates," *IEEE MTT-S Int. Microw. Symp. Dig.*, pp. 12–14, 2012, doi: 10.1109/MWSYM.2012.6259668.

[8] J. A. Yeh, C. A. Chang, C. C. Cheng, J. Y. Huang, and S. S. H. Hsu, "Microwave characteristics of liquid-crystal tunable capacitors," *IEEE Electron Device Lett.*, vol. 26, no. 7, pp. 451–453, 2005, doi: 10.1109/LED.2005.851118.

[9] K. Nomura, H. Ohta, A. Takagi, T. Kamiya, M. Hirano, and H. Hosono, "Room-temperature fabrication of transparent flexible thin-film transistors using amorphous oxide semiconductors," *Nature*, vol. 432, no. 7016, pp. 488–492, 2004, doi: 10.1038/nature03090.

[10] Sharp Corporation, "Sharp Begins Production of Worlds First LCD Panels Incorporating IGZO Oxide Semiconductors," *Press Release*, April 13, 2012, URL: http://www.sharp-world.com/corporate/news/120413.html.

[11] K. Hachisuka, Y. Terauchi, Y. Kishi, K. Sasaki, T. Hirota, H. Hosaka, K. Fujii, M. Takahashi, and K. Ito, "Simplified circuit modeling and fabrication of intrabody communication devices," *Sensors Actuators, A Phys.*, vol. 130–131, no. SPEC. ISS., pp. 322–330, 2006, doi: 10.1016/j.sna.2006.04.044.

[12] E. Hegazi and A. A. Abidi, "Varactor characteristics, oscillator tuning curves, and AM-FM conversion," *IEEE J. Solid-State Circuits*, vol. 38, no. 6, pp. 1033–1039, 2003, doi: 10.1109/JSSC.2003.811968.

[13] A. Mahmud, T. S. Kalkur, A. Jamil and N. Cramer, "A 1-GHz active phase shifter with a ferroelectric varactor," *IEEE Microw. Wirel. Components Lett.*, vol. 16, no. 5, pp. 261–263, 2006, doi: 10.1109/LMWC.2006.873529.

[14] S. Knobelspies, A. Daus, G. Cantarella, L. Petti, N. Münzenrieder, G. Tröster, G. A. Salvatore, "Flexible a-IGZO Phototransistor for Instantaneous and Cumulative UV-Exposure Monitoring for Skin Health", *Adv. Electron. Mater.*, vol. 2, no. 10, p. 1600273, 2016, doi: 10.1002/aelm.201600273.

[15] A. Daus, C. Vogt, N. Münzenrieder, L. Petti, S. Knobelspies, G. Cantarella, M. Luisier, G. A. Salvatore, and G. Tröster, "Positive charge trapping phenomenon in n-channel thin-film transistors with amorphous alumina gate insulators", *J. Appl. Phys.*, vol. 120, no. 24, p. 244501, 2016, doi: 10.1063/1.4972475.

[16] R. Martins, A. Nathan, R. Barros, L. Pereira, P. Barquinha, N. Correia, R. Costa, A. Ahnood, I. Ferreira, and E. Fortunato, "Complementary metal oxide semiconductor technology with and on paper," *Adv. Mater.*, vol. 23, no. 39, pp. 4491–4496, 2011, doi: 10.1002/adma.201102232.

[17] R. Lindner, "Semiconductor Surface Varactor," *Bell Syst. Tech. J.*, vol. XLI, no. 3, pp. 805–831, 1962, doi: 10.1002/j.1538-7305.1962.tb00477.x.

[18] J. Zhang,Y. Li, B. Zhang, H. Wang, Q. Xin, A. Song, "Flexible indium-gallium-zinc-oxide Schottky diode operating beyond 2.45 GHz," *Nat. Commun.*, vol. 6, no. 5, pp. 7561, 2015, doi: 10.1038/ncomms8561.

[19] M. D. Groner, J. W. Elam, F. H. Fabreguette, S. M. George, "Electrical characterization of thin Al2O3 films grown by atomic layer deposition on silicon and various metal substrates," *Thin Solid Films*, vol. 413, no. 1-2, pp. 186–197, 2002, doi: 10.1016/S0040-6090(02)00438-8.

[20] H. Bae, S. Jun, C. H. Jo, H. Choi, J. Lee, Y. H. Kim, S. Hwang, H. K. Jeong, I. Hur, W. Kim, D. Yun, E. Hong, H. Seo, D. H. Kim, and D. M. Kim, "Modified conductance method for extraction of subgap density of states in a-IGZO thin-film transistors," *IEEE Electron Device Lett.*, vol. 33, no. 8, pp. 1138–1140, 2012, doi: 10.1109/LED.2012.2198870.

[21] A. Bhoolokam, M. Nag, A. Chasin, S. Steudel, J. Genoe, G. Gelinck, G. Groeseneken, and P. Heremans, "Analysis of frequency dispersion in amorphous InGaZnO thin-film transistors," *J. Inf. Disp.*, vol. 16, no. 1, pp. 31–36, 2014, doi: 10.1080/15980316.2014.991769.

[22] N. Münzenrieder, L. Petti, C. Zysset, T. Kinkeldei, G. A. Salvatore, G. Tröster, "Flexible self-aligned amorphous InGaZnO thin-film transistors with submicrometer channel length and a transit frequency of 135 MHz", *IEEE Trans. Electron Devices*, vol. 60, no. 9, pp. 1–6, 2013, doi: 10.1109/TED.2013.2274575.